Journal of Applied and Natural Science
18(1), 279 - 292 (2026)
ISSN : 0974-9411 (Print), 2231-5209 (Online)
journals.ansfoundation.org

Research Article

Carbon supported $Fe_{70}Co_{20}Ni_{10}$ trimetallic catalyst for enhanced cathode performance in Dual-chamber microbial fuel cells for wastewater treatment

Pournan L
Department of Microbiology and Biotechnology, Presidency College (Autonomous), University of Madras, Chennai- 600005, India
Sasikala S*
Department of Microbiology and Biotechnology, Presidency College (Autonomous), University of Madras, Chennai- 600005, India

*Corresponding author. E-mail: drsasikalas6@gmail.com

Article Info
https://doi.org/10.31018/jans.v18i1.7091
Received: August 09, 2025
Revised: February 17, 2026
Accepted: February 25, 2026

How to Cite
Pournan L and Sasikala S (2026). Carbon supported $Fe_{70}Co_{20}Ni_{10}$ trimetallic catalyst for enhanced cathode performance in Dual-chamber microbial fuel cells for wastewater treatment. *Journal of Applied and Natural Science*, 18(1), 279 - 292. https://doi.org/10.31018/jans.v18i1.7091

Abstract
Scalable microbial fuel cells (MFCs) for simultaneous wastewater treatment and electricity generation require cost-effective, high-performance cathode catalysts that operate efficiently at neutral pH. Herein, the present study reports a trimetallic $Fe_{70}Co_{20}Ni_{10}$ alloy nanoparticle catalyst supported on carbon ($Fe_{70}Co_{20}Ni_{10}$/C) as a highly active and durable oxygen reduction reaction (ORR) electrocatalyst. The catalyst was synthesized via a facile thermal-activation route using sodium borohydride ($NaBH_4$), yielding homogeneous alloy nanoparticles (8–12 nm) with pronounced electron transfer from Fe to Ni, thereby optimizing oxygen adsorption energy and enhancing ORR kinetics. When deployed as a cathode in a dual-chamber MFC at 1.0 mg cm^{-2} loading, $Fe_{70}Co_{20}Ni_{10}$/C delivered a maximum power density of 1532 mW m^{-2} and an open-circuit voltage of 0.936 V, and operational stability for over 1100 hours. This configuration also achieved high wastewater treatment efficiency, with 89.7% chemical oxygen demand (COD) removal and 9.7% coulombic efficiency. These findings highlight the superior catalytic and operational performance of $Fe_{70}Co_{20}Ni_{10}$/C compared with the synthesized mono- and bimetallic Fe, Co, and Ni-based catalysts, suggesting its potential as a cost-effective alternative to precious-metal catalysts for MFC applications for wastewater treatment.

Keywords: Coulombic efficiency, Dual-chamber microbial fuel cell reactor, $Fe_{70}Co_{20}Ni_{10}$/C cathode catalyst, Oxygen reduction reaction (ORR), Power density

INTRODUCTION

The increasing intensity of environmental pollution and the energy crisis have led the investigators to explore sustainable, renewable methods for next-generation energy conversion and storage technologies. Microbial fuel cell reactor (MFCR) has emerged as a propitious technology for addressing both environmental pollution and energy scarcity (Soleimani *et al*., 2023; Mohammadi *et al*., 2023). These bio-electrochemical devices operate by harnessing the metamorphic activity of microorganisms to decompose organic pollutants in water while simultaneously generating electricity (Pan *et al*., 2023). In a dual-chamber MFCR, the anode hosts microbial communities that break down organic matter, releasing electrons and protons. These charge carriers are transferred to the cathode, where they participate in the oxygen reduction reaction (ORR) (Khater *et al*., 2024). Most MFCRs are operated at neutral pH to support optimal bacterial growth. However, these conditions pose a challenge for power generation, as the low hydrogen ion (H^+) concentration leads to sluggish ORR kinetics. In this context, the cathode catalyst plays a pivotal role in determining MFC performance, as it directly influences the rate of electrical current production through the ORR (Pan *et al*., 2022; Scharf *et al*., 2022). Although platinum-based materials have long been favored due to their ability to reduce overpotential and enhance ORR kinetics, their high cost, limited stability, and susceptibility to poisoning hinder their practical and sustainable application in MFCR (Nandikes *et al*., 2022). As a result, significant research efforts have been dedicated to developing low-cost, stable, and efficient alternative electrocatalysts to replace platinum,

thereby improving MFC performance and facilitating broader implementation in wastewater treatment and renewable energy generation (Dessie *et al*., 2022).

Recent advancements in transition metal alloys have significantly improved their chemical and electronic properties, particularly in the development of non-precious iron (Fe)-based electrocatalysts to enhance electrooxidation kinetics (Zhou *et al*., 2020). However, Fe and Fe/Fe_3C nanoparticles have demonstrated potential as functional sites for the oxygen reduction reaction (ORR), Fe supported catalysts in MFCR face several limitations, including poor stability, iron leaching, and diminished ORR activity under neutral pH conditions (Gangadharan *et al*., 2021). To address these challenges, researchers have explored incorporating cobalt (Co) into Fe-based catalysts. The addition of Co induces a lower spin state in the iron center, which facilitates OH desorption and enhances ORR kinetics. Although bimetallic Fe–Co catalysts exhibit improved performance, they still encounter issues such as limited stability at neutral pH, incomplete oxygen reduction, and the formation of reactive intermediates that compromise efficiency and durability (Ma *et al*., 2021).

To overcome these limitations, a trimetallic approach involving the incorporation of nickel (Ni) into Fe–Co catalysts has been investigated. The addition of Ni has shown to significantly enhance ORR activity, catalytic stability, and electron transfer efficiency in MFCR. Moreover, Ni promotes the favorable 4-electron ORR pathway, thereby reducing harmful peroxide formation and improving overall catalytic performance (Wang *et al*., 2023). This trimetallic strategy allows precise tuning of the adsorption potency and arrangement of ORR intermediates on the catalyst surface, offering a more effective approach than mono- and bimetallic systems for achieving superior intrinsic ORR activity. Therefore, developing FeCoNi trimetallic catalysts for the cathode represents a promising strategy to enhance ORR performance in microbial fuel cells (Liu *et al*., 2019).

Here, a series of trimetallic ORR catalysts comprising Fe, Co, and Ni was prepared by retorting a variety of these metals in a nitrogen (N_2) atmosphere. The study revealed that altering the Fe-to-Ni atomic ratio induced electron reallocation, with electrons transferring from Fe to Ni. This electron transfer played a prominent role in enhancing the catalytic activity of the trimetallic approach (Mercado *et al*., 2020). To address practical demands, forming a trimetallic alloy of Fe-Co-Ni on carbon substrates ensures excellent electrical conductivity and stability, positioning it as an efficient and economical electrocatalyst for slow electrooxidation processes. Experimental results emphasized the importance of embedded metal fragments and demonstrated the catalytic advantages of the trimetallic composition in improving ORR efficiency.

The carbon doped trimetallic catalyst exhibited superior performance compared to its mono- and bimetallic counterparts, primarily due to its interconnected network structure, which exposed a greater number of active sites and enhanced overall catalytic activity (Bhat *et al*., 2024). Overall, the synthesized catalysts $Fe_{70}Co_{20}Ni_{10}$/C showed the highest ORR activity, attributed to its amended inherent properties and increased electrochemically dynamic surface area. Notably, when applied in MFCR, the $Fe_{70}Co_{20}Ni_{10}$ /C cathodic catalyst delivered a power density comparable to other reported non-precious-metal catalysts and commercially available Fe-, Co-, or Ni-based catalysts, while also exhibiting improved long-term stability. These findings underscore the potential of $Fe_{70}Co_{20}Ni_{10}$ /C trimetallic catalysts as cost-effective and efficient replacements to invaluable metal-supported catalysts for ORR invocations in sustainable energy systems (Jadhav *et al*., 2024; Zhao *et al*., 2019). This study aimed to create a low-cost and durable $Fe_{70}Co_{20}Ni_{10}$ alloy catalyst on carbon that improves oxygen reduction in dual-chamber microbial fuel cells working at neutral pH. It focuses on optimizing the catalyst's makeup and structure to boost its activity, stability, and ability to treat wastewater. The goal was to offer an effective non-precious-metal alternative to platinum catalysts for sustainable electricity generation and wastewater cleaning.

MATERIALS AND METHODS

Synthesis of Fe-Co-Ni/C Catalysts

The assimilation of Fe-Co-Ni trimetallic catalysts involves a dual-phase reduction strategy that combines chemical and heat treatments. Initially, hydrated nickel nitrate, ferric nitrate, and cobalt nitrate salts are disintegrated into deionized water and mixed with Vulcan XC-72R carbon powder. The mixture is sonicated for 30 minutes to ensure uniform dispersion and then stirred at 60 °C for 20 minutes. A 1 M $NaBH_4$ solution is augmented to minimize the metal ions to their elemental states. The resulting catalyst predecessor is purified, washed with deionized water, and desiccated in a kiln about 60 °C for the sake of an hour. In the second stage, thermal reduction is carried out by treating the dried precursor under a hydrogen gas flow at 800 °C for 10 hours to obtain Fe-Co-Ni trimetallic catalysts. An identical synthesis protocol was used to produce Fe/C, Fe-Co/C, and Fe-Ni/C catalysts, with variations only in the Fe, Co, and Ni molar ratios. Each catalyst had a 40:60 metal-to-carbon weight ratio (Dey *et al*., 2020).

Physical characterization

The crystalline arrangement of the synthesized cathodic catalysts was examined using X-ray diffractometer furnished with a wavelength of 0.154 nm of Cu Kα radiation source. The surface morphology of the prepared catalysts was scrutinized by means of a scanning elec-

tron microscope (Zeiss Ultra Plus) operated at 15 kV expedited voltage. X-ray photoelectron spectrometry is primarily used to analyze the elemental composition and electronic states of synthesized catalysts (Xie *et al*., 2017).

Electrochemical characterization

Electrochemical studies were carried out on a CHI-6005E SN1077 workstation using a three-electrode cell. The working electrode was prepared by dispersing a catalyst (5 mg) in a 0.25 wt% Nafion-ethanol solution (3 ml), followed by ultrasonication for 2 hours. A 20 µL aliquot of consequential ink was added to a pre-polished glassy carbon electrode (0.196 cm²), resulting in a catalyst loading of 0.40 mg/cm². Oxygen reduction reaction (ORR) activity was assessed using linear sweep voltammetry (LSV) at 10 mV/s across rotation speeds of 625–2025 rpm (Subhadarshini *et al*., 2023). All electrochemical measurements were performed in triplicate, and results are reported as mean ± standard deviation. Cyclic voltammetry (CV) was used to determine the double-layer capacitance (C_{dl}), which served as the basis for estimating the electrochemically active surface area (ECSA). The C_{dl} was derived from equation (1):

$$C_{dl} = i_c/v \quad (1)$$

Here, i_c - charge current density and

v is the scan rate

The ECSA was then calculated using the equation (2):

$$ECSA = C_{dl}/C_s \quad (2)$$

C_s - specific capacitance

Power density and polarization curves are key characterization techniques for evaluating the electrogenesis capacity of sediment-based MFCRs. These measurements are taken once the voltage output stabilizes at its peak. A range of external resistances (34,000 to 52 Ω) is applied in descending order, with each allowed a 10-minute stabilization period. Anode and cathode potentials are then recorded with a digital multimeter using a saturated Ag/AgCl (2 M KCl) electrode as the reference (Ishaq *et al*., 2024).

Chemical Oxygen Demand (COD) is a key characterization technique for evaluating the organic load in wastewater and the treatment efficiency of sediment-based microbial fuel cell reactor. COD values are measured at both the start and end of the operational cycle using a commercial COD detector, and the removal efficiency is calculated to assess the degradation of organic matter (Tornheim *et al*., 2020). All COD removal and coulombic efficiency measurements were performed in three independent experimental runs (n = 3), and results are reported as mean ± standard deviation. This parameter is essential for understanding the MFCR performance in wastewater treatment. The values of COD was calculated using equation (3):

$$\text{COD removal efficiency (\%)} = COD_1 - COD_2 / COD_1 \times 100\ \% \quad (3)$$

Here, COD_1 and COD_2 represent the COD concentrations at the start and termination of the batch-fed process, respectively.

Coulombic efficiency (CE) is another critical metric that reflects the proportion of electrons from substrate oxidation that are captured as electrical current. It was calculated using the equation (4):

$$CE = M \int_0^{tb} Idt \,/\mathrm{FbV}anode\Delta COD \quad (4)$$

Herein, M - Oxygen molecular weight (32 g/mol),

F - Faraday's constant with a value of 96,485 C/mol,

b - number of electrons associated with per mole of oxygen (4),

V_{anode} - substrate solution volume (28 mL), and

ΔCOD - COD changes during the period t_b.

This approach enables accurate evaluation of electrochemical efficiency and supports optimization of MFCR configurations and operating conditions.

Assembling and operation of the dual-chamber Microbial fuel cell reactor (MFCR)

The microbial fuel cell reactor (MFCR) is an advanced dual-chamber system designed for the efficient generation of bioelectricity (Fig. 1) (Tan *et al*., 2020). It adopts an upflow configuration with a total working volume of 620 ml, comprising a 315 ml anoxic anodic chamber and a 305 ml oxic cathodic chamber. During operation, the influent is introduced at the bottom of the anodic section and dwells from the top of the cathodic section, ensuring a persistent upward flow. A polypropylene pad is employed as a separator membrane to facilitate proton exchange while maintaining physical separation between the chambers. The reactor temperature is maintained under ambient room conditions using an Inkbird ITC-1000 controller to ensure operational stability. Each chamber is equipped with two electrode assemblies, each consisting of 10 graphite rods measuring 55 mm in length and 3 mm in diameter. The rods are spaced 1.5 mm apart to maximize surface area exposure. Each electrode assembly provides an overall surface coverage of 119.3 cm² and occupies a space of 5 cm³. The anode, comprising graphite rods, is placed in the anaerobic chamber filled with inoculated wastewater to promote the growth and activity of electrogenic microorganisms. The cathode, also made of graphite, was modified with a FeCoNi/C trimetallic catalyst, prepared by dispersing the catalyst in ethanol with a Nafion binder, then drop-casting it onto the electrode. This modified cathode is installed in the oxic chamber, continuously aerated to support the oxygen reduction reaction (ORR). Both electrodes were externally connected through a conductive wire and a resistor to enable real-time monitoring of voltage and current.

Fig. 1. *Schematic representation of the Microbial fuel cell reactor*

The entire system is hermetically sealed to preserve anoxic conditions in the anodic section and oxygen-rich conditions in the cathodic section. For controlled oxygen delivery, sodium perborate ($NaBO_3 \cdot 4H_2O$) is utilized as a solid oxygen-releasing agent (Gayathri *et al*., 2022). A dedicated delivery unit is positioned at the top of the cathodic chamber to administer the compound. Sodium perborate, a stable solid precursor of hydrogen peroxide, hydrolyzes upon dissolution to release H_2O_2, as shown in equation (5). This method ensures safer handling, accurate dosing, and improved storage stability when compared to liquid peroxide, making it well-suited for prolonged operation. A peristaltic pump was used to deliver the H_2O_2 solution at a constant flow rate of 10.8 ml/h, ensuring uniform, controlled dosing throughout the process.

$$[B(OH)_3(O_2H)]^- + H_2O \rightleftharpoons [B(OH)_4]^- + H_2O_2 \quad (5)$$

During reactor operation, electrogenic microbes at the anode break down organic matter, producing electrons that are transmitted to the cathode via an external circuit. The anode was fed with inoculated wastewater prepared by mixing activated sludge with synthetic wastewater (1:1 v/v) adjusted to COD 4321 ± 50 mg/L. The inoculated wastewater used in this study was collected from a municipal sewage treatment facility in Chennai, India. Its initial characteristics were: COD = 4321 ± 115 mg/L, BOD_5 = 1986 ± 74 mg/L, pH = 7.2 ± 0.1, conductivity = 1.34 ± 0.05 mS/cm, and total suspended solids = 612 ± 28 mg/L. The wastewater contained its native mixed microbial consortium without external inoculum. Prior to use, coarse particulates were removed by sieving through a 1 mm mesh, and the sample was stored at 4 °C for no longer than 48 hours. The synthetic feed (per L) contained glucose, acetate, peptone, NH_4Cl, KH_2PO_4/K_2HPO_4, $MgSO_4 \cdot 7H_2O$, $CaCl_2$, and trace metals. The MFCR was conditioned for 30 days at 30°C until a stable biofilm formed. For reproducibility, each batch of feed followed the same recipe and COD check; temperature, hydraulic conditions, and biofilm were kept constant, and only the cathode was replaced. Cycle consistency was confirmed by COD (<±5%), CE (<±0.5%), and voltage (<±10 mV) variation. In the cathodic region, oxygen undergoes reduction in the presence of Fe-based carbon-doped catalysts, thereby generating electricity. Throughout the operation, sodium perborate did not significantly affect the cathodic environment. The cathode pH remained stable (6.8–7.2), indicating that the slow hydrolysis of sodium perborate did not cause measurable acidification or alkalinization. No accumulation of H_2O_2 was detected, as the $Fe_{70}Co_{20}Ni_{10}$ /C catalyst predominantly favors a 4-electron ORR pathway. Furthermore, stable OCV and polarization behavior over 1100 hours confirmed the absence of catalyst poisoning or surface deactivation. Although sodium perborate releases small amounts of H□O□ during hydrolysis, the predominant oxidant at the cathode is molecular oxygen generated in situ. The cathodic reaction therefore remains O□ reduction rather than hydrogen peroxide reduction. No measurable H□O□ accumulation was observed, and stable long-term cathodic performance confirms that ORR is the dominant pathway. Accordingly, LSV in an O□-saturated electrolyte accurately represents the catalyst's behavior under operating conditions. The reactor's performance is evaluated using parameters such as open-circuit voltage (OCV) and power density, and

electrochemical methods including cyclic voltammetry and electrochemical impedance spectroscopy. Routine maintenance, such as replenishing the nutrient medium and inspecting electrode integrity, is essential for ensuring stable, efficient reactor operation.

RESULTS AND DISCUSSION

Physical characterization

The XRD analysis of $Fe_{70}Co_{20}Ni_{10}$/C reveals a face-centered cubic (fcc) structure with characteristic peaks slightly shifted to higher angles compared to Fe□□□/C, indicating lattice contraction due to Co and Ni incorporation. This confirms successful alloying and formation of a homogeneous Fe–Co–Ni solid solution without separate Co or Ni phases, demonstrating good miscibility and structural uniformity. These findings align with prior studies reporting similar lattice contractions and phase formation in Fe-based trimetallic alloys. For instance, (Theofanidis *et al*., 2018) observed that alloying Fe with transition metals like Co and Ni induces lattice distortions consistent with enhanced catalytic properties. Similarly, (Muthusamy *et al*., 2023) reported that homogeneous alloy formation in Fe-Co-Ni systems contributes to improved electronic structure and catalytic activity, as no separate metallic phases were detected by XRD. The absence of distinct Co or Ni crystalline peaks supports the formation of a solid solution rather than phase segregation, which is crucial for synergistic electronic effects that enhance ORR kinetics, as discussed by (Sawant *et al*., 2016). This structural uniformity facilitates electron redistribution (notably Fe to Ni transfer), which linked to optimized oxygen adsorption and improved catalytic performance. Overall, the XRD results corroborate the catalytic improvements observed electrochemically and structurally in this study, consistent with the literature emphasizing the importance of alloy homogeneity and lattice modulation in enhancing ORR activity and stability in neutral pH microbial fuel cell cathodes.

The scanning electron microscope (SEM) analysis revealed intricate morphological features of the prepared catalysts. The SEM images of Fe_{100}/C, $Fe_{70}Co_{30}$/C, $Fe_{70}Ni_{30}$/C and $Fe_{70}Co_{20}Ni_{10}$/C (Fig. 3a–d) showed uniform metal dispersion within the doped carbon matrix, indicating effective synthesis without noticeable agglomeration (Luo *et al*., 2021). This homogeneous distribution enhances the catalytic surface area and reactivity. To enable direct morphological comparison, an additional set of SEM images for all catalysts was obtained at a uniform magnification. These standardized micrographs have been included, and it allowing clearer assessment of particle dispersion, surface texture, and agglomeration behavior across catalyst compositions. The carbon support appeared to anchor the metal particles, contributing to structural stability. These

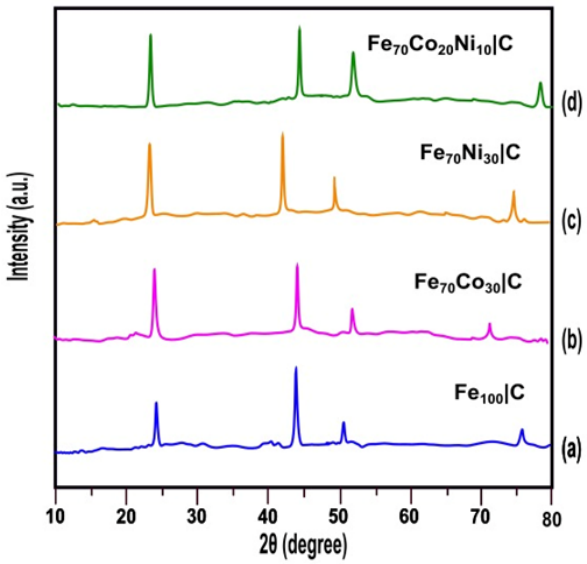

Fig. 2. *XRD profiles of* ***(a)*** *Fe_{100}/C,* ***(b)*** *$Fe_{70}Co_{30}$/C,* ***(c)*** *$Fe_{70}Ni_{30}$/C,* ***(d)*** *$Fe_{70}Co_{20}Ni_{10}$/C catalysts*

morphological insights correlate strongly with the catalysts expected electrochemical performance in microbial fuel cell applications.

Energy dispersive X-ray Spectroscopy (EDX) was used to characterize the elemental composition of the synthesized catalysts. EDX spectra, (Fig. 4a–d), confirmed the presence of various elements, including Fe, Co, Ni, and carbon, depending on the specific catalyst formulation (Gilanizadeh *et al*., 2018). As summarized in (Table 1), the quantitative analysis provided detailed insights into the elemental distribution within the catalysts. The results indicated that the intended elements were successfully incorporated into the catalyst matrices and were uniformly distributed on the carbon supports. This uniform dispersion is critical for enhancing the chemical reactivity and overall behavior of the functional materials. Minor variations in elemental composition were observed, which can be attributed to the synthesis process. These variations, however, remained within acceptable limits, suggesting that the preparation method was effective in achieving the desired composition while minimizing material losses.

An XPS study was carried out to explore the chemical environments present in the catalysts. In (Fig. 5), the XPS profiles of Fe_{100}/C, $Fe_{70}Co_{30}$/C, $Fe_{70}Ni_{30}$/C, and $Fe_{70}Co_{20}Ni_{10}$/C are illustrated (Fantauzzi *et al*., 2019). The high-resolution Fe 2p spectra (Fig. 5a and 5b) exhibited characteristic peaks in the ranges of 704.0–719.0 eV and 722.0–734.0 eV. The Fe $2p_{3/2}$ peaks of $Fe_{70}Co_{20}Ni_{10}$/C and Fe_{100}/C were deconvoluted into Fe^0 (704.2–712.4 eV), Fe^{2+} (709.1–712.4 eV), and Fe^{3+} (714.2–715.2 eV) species. Similarly, the Fe $2p_{1/2}$ peaks were resolved into Fe^0 (716.2–721.3 eV), Fe^{2+} (721.3–725.5 eV), and Fe^{3+} (724.8–733.2 eV) components. The Co 2p spectra (Fig. 5c and 5d) for $Fe_{70}Co_{20}Ni_{10}$/C and Co_{100}/C exhibited peaks at 779.3–784.3 eV and

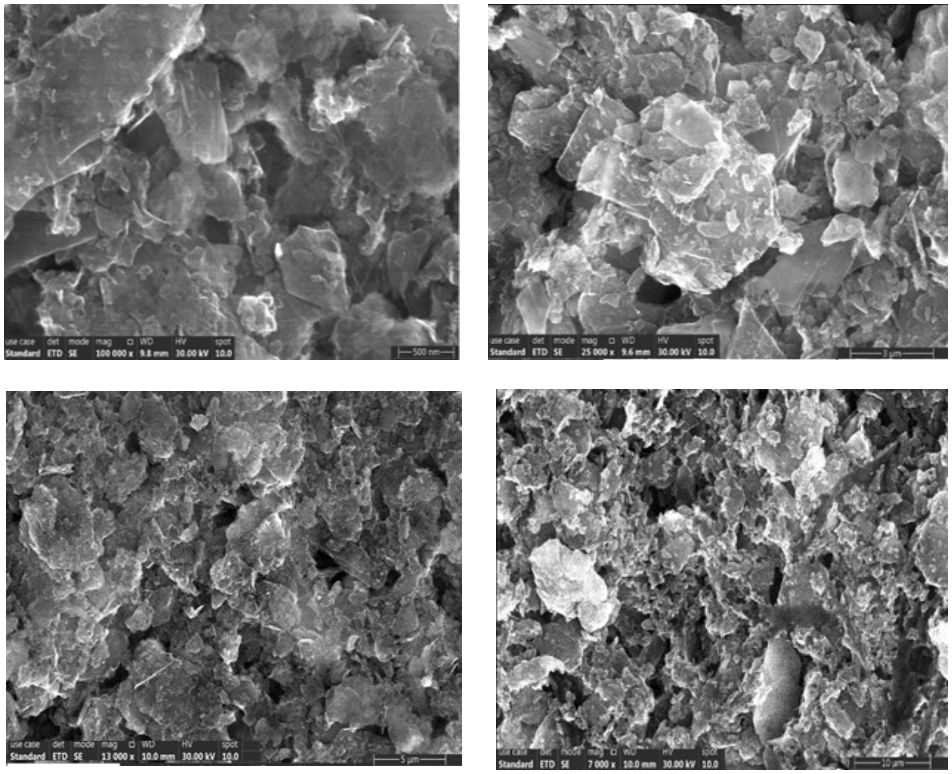

Fig. 3. *Scanning electron microscopic images of* ***(a)*** Fe_{100}/C, ***(b)*** $Fe_{70}Co_{30}/C$, ***(c)*** $Fe_{70}Ni_{30}/C$, ***(d)*** $Fe_{70}Co_{20}Ni_{10}$***/C catalysts***

793.7–780.0 eV, corresponding to Co $2p_{3/2}$ and Co $2p_{1/2}$, respectively, which were further deconvoluted into Co^0, Co^{2+}, and Co^{3+} species. (Fig. 5e and 5f) highlight Ni spectra from $Fe_{70}Co_{20}Ni_{10}$/C and Ni_{100}/C, where peaks appeared at 854.2–855.0 eV and 872.3–875.2 eV, attributed to Ni $2p_{3/2}$ and Ni $2p_{1/2}$, which were deconvoluted into Ni^0, Ni^{2+}, and higher oxidation states. Notably, a positive shift in the Fe^{3+} peak was observed for $Fe_{70}Co_{20}Ni_{10}$/C (715.7 eV) compared to Fe_{100}/C (714.3 eV), indicating electron transfer, likely from Fe to Ni, as the Ni content increased. The XPS results clearly support electron transfer from Fe to Ni. A +1.4 eV shift in the Fe^{3+} $2p_{3/2}$ peak (715.7 eV in $Fe_{70}Co_{20}Ni_{10}$/C vs. 714.3 eV in Fe_{100}/C) indicates decreased electron density on Fe. Correspondingly, the Ni $2p_{3/2}$ peak appears slightly stabilized (854.2–855.0 eV), showing increased electron density on Ni. The higher proportion of Fe^{3+} species in the alloy further confirms Fe oxidation due to electron loss. Together, these binding energy shifts and changes in oxidation-state distribution provide strong evidence for electron transfer from Fe to Ni, which, in turn, contributes to the enhanced electronic conductivity and improved ORR catalytic activity of the $Fe_{70}Co_{20}Ni_{10}$/C catalyst. This electron redistribution likely lowers the Fe d-band re, weakening the excessively strong OH adsorption and enabling faster intermediate desorption, a well-established factor that contributes to improved ORR kinetics in Fe–Ni–based catalysts. This electron redistribution is expected to enhance electron conductivity and improve the electrocatalytic performance toward the oxygen reduction reaction (ORR). Furthermore, by varying the Fe-Co-Ni atomic ratio, the electronic structure is optimized to regulate the interaction and turnover of oxygen-derived species, thus significantly elevating oxygen reduction catalytic activity.

Electrochemical characterization

The addition of Co and Ni to the Fe precursor was found to enhance the ORR electrocatalytic activity, revealing significant differences in catalytic performance. Linear sweep voltammetry (LSV) confirmed that all synthesized catalysts exhibited ORR activity, with distinct variations in measured currents at a fixed electrode rotation rate, indicating differences in catalytic efficiency (Zhong *et al*., 2020). As seen in (Fig. 6a), the LSV profiles exhibited a region governed by both kinetic and diffusion processes from 0.5 to 1.0 V, with a subsequent plateau below 0.5 V indicating diffusion-limited behavior. Among the evaluated catalysts, $Fe_{70}Co_{20}Ni_{10}$/C exhibited the best ORR activity, achieving an Eonset of 0.944 V and an $E_{1/2}$ of 0.823 V at 1225 rpm, as shown in (Fig. 6b). This catalyst outperformed the bimetallic $Fe_{70}Co_{30}$/C (0.902 V and 0.781 V), $Fe_{70}Ni_{30}$/C (0.837 V and 0.748 V), and the monometallic Fe_{100}/C (0.801 V and 0.726 V) counterparts, as shown in (Fig. 6c), highlighting the advantage of incorporating multiple metals. The observed improvement in catalytic activity with the addition of Co and Ni to Fe demonstrates a clear synergistic effect. These included monometallic

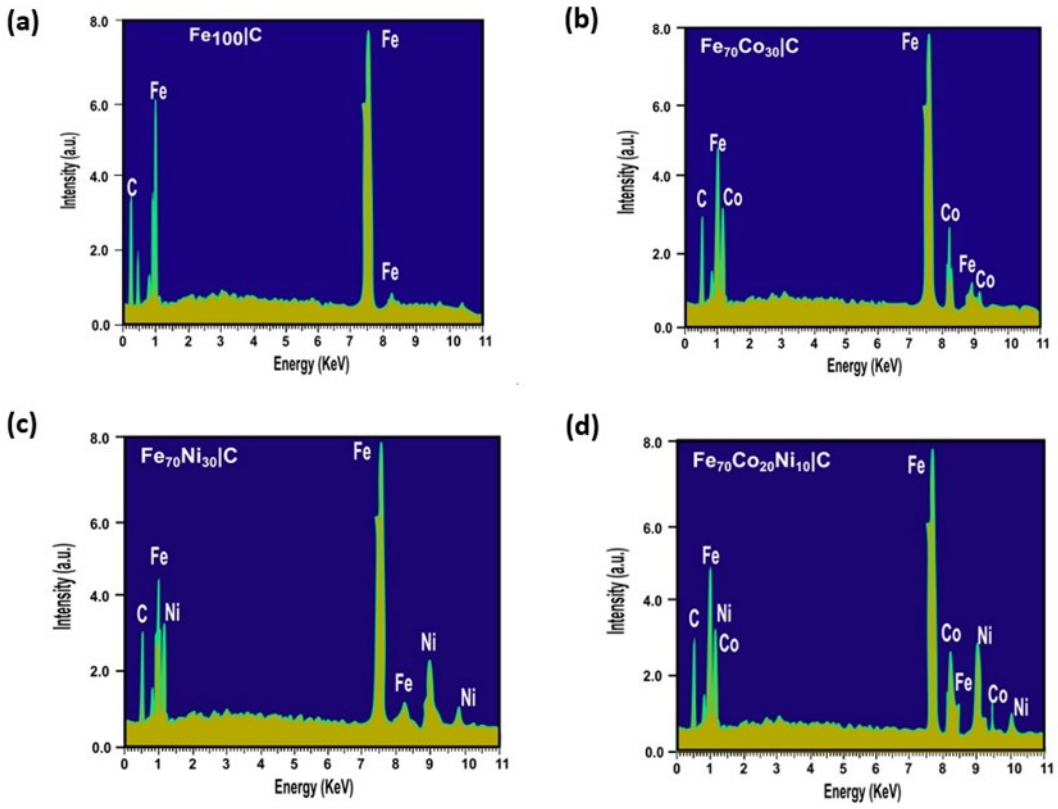

Fig. 4. *EDX spectra of* ***(a)*** Fe_{100}/C, ***(b)*** $Fe_{70}Co_{30}/C$, ***(c)*** $Fe_{70}Ni_{30}/C$, ***(d)*** $Fe_{70}Co_{20}Ni_{10}/C$ *catalysts*

Table 1. EDX values of Fe_{100}/C, $Fe_{70}Co_{30}/C$, $Fe_{70}Ni_{30}/C$ and $Fe_{70}Co_{20}Ni_{10}/C$ catalysts

Catalysts	Ratio in dosage			Ratio in product		
	Fe	Co	Ni	Fe	Co	Ni
Fe_{100}/C	100	-	-	100	-	-
$Fe_{70}Co_{30}/C$	70	30	-	73	27	-
$Fe_{70}Ni_{30}/C$	70	-	30	72	-	28
$Fe_{70}Co_{20}Ni_{10}/C$	70	20	10	71	18	11

Fe_{100}/C, bimetallic $Fe_{70}Co_{30}/C$ and $Fe_{70}Ni_{30}/C$, as well as several preliminary Fe–Co–Ni combinations. Among all tested formulations, the 70:20:10 Fe:Co:Ni ratio consistently delivered the best performance, with the highest onset potential (0.944 V), the highest kinetic current density (2.83 mA/cm²), and the largest ECSA. Other ratios resulted in lower ORR activity or less stable electron distribution. Thus, the $Fe_{70}Co_{20}Ni_{10}/C$ composition was selected because it provided the most favorable synergistic interaction, optimized electron transfer (particularly Fe→Ni), and superior catalytic performance compared to the other tested ratios. The bimetallic catalysts displayed intermediate performance, whereas Fe_{100}/C exhibited the lowest E_{onset} and $E_{1/2}$ values (Table 2). This suggests that the incorporation of a second and third metal significantly magnifies the electrocatalytic function of the monometallic Fe stimulant. Overall, aforementioned observed improvements during ORR activity underscore the importance of optimizing the Fe, Co, and Ni proportions to design efficient electrocatalysts for oxygen reduction reactions.

To further probe the electrocatalytic properties, the kinetic current density (J_K) was resolute from the Koutecky–Levich (K–L) plots (Fig. 6d) (Guadarrama-Pérez *et al*., 2023). The half-wave potential for all the catalysts was centered around 0.8 V. At the potential 0.8 V (vs. RHE), the current is dominated by the kinetics of the ORR, making it suitable for calculating J_K. The obtained J_K values at 0.8 V were 1.57 mA/cm² for Fe_{100}/C, 1.73 mA/cm² for $Fe_{70}Ni_{30}/C$, 1.84 mA/cm² for $Fe_{70}Co_{30}/C$, and 2.83 mA/cm² for $Fe_{70}Co_{20}Ni_{10}/C$ (Fig. 6c). These results reveal that J_K is strongly dependent on the Fe–Ni ratio, with the trimetallic composition showing the most pronounced enhancement.

To investigate the inherent ORR performance of the catalysts, their electrochemically active surface areas (ECSA) were determined using cyclic voltammetry (Fig. 7) (Zhang *et al*., 2024). The $Fe_{70}Co_{20}Ni_{10}/C$ catalyst ex-

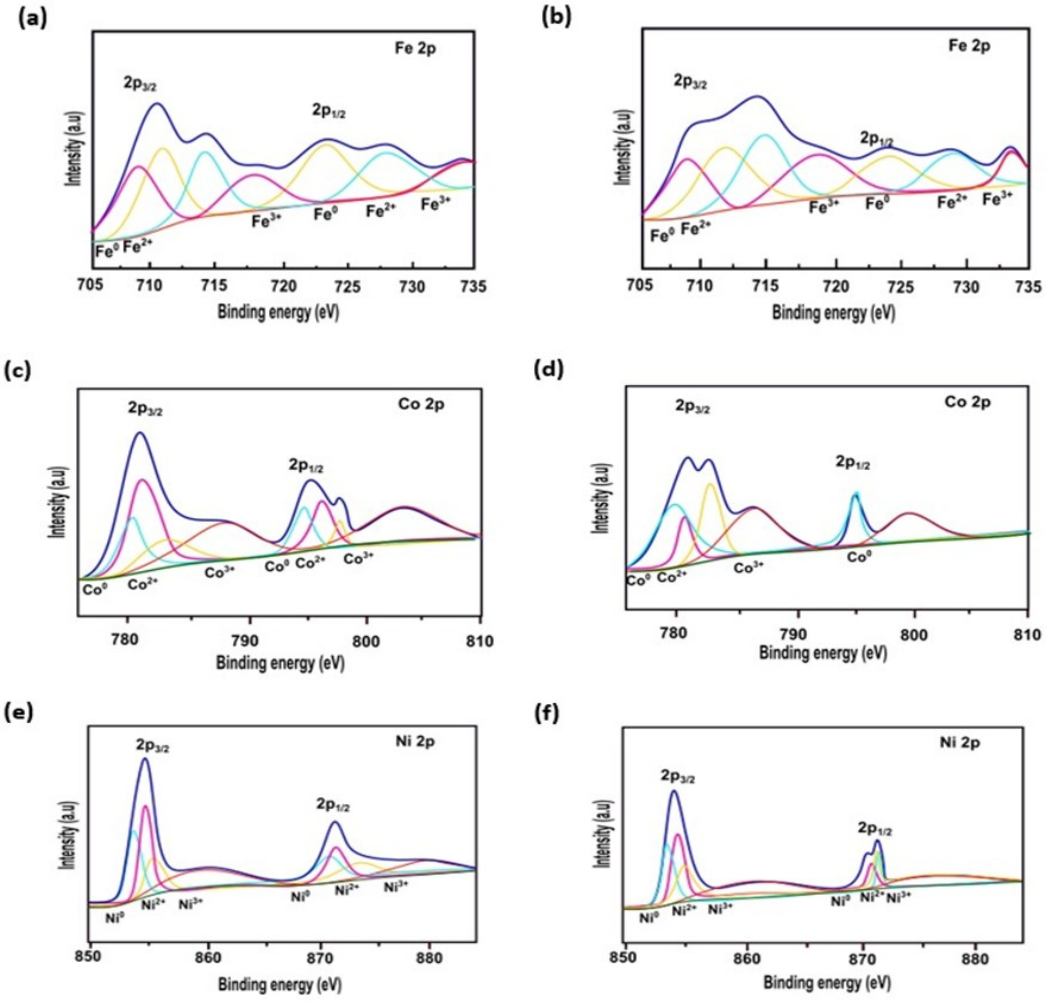

Fig. 5. ***(a, b)*** *XPS spectra of Fe 2p of* $Fe_{70}Co_{20}Ni_{10}$*/C and* Fe_{100}*/C,* ***(c, d)*** *XPS spectra of Co 2p of* $Fe_{70}Co_{20}Ni_{10}$*/C and* Co_{100}*/C,* ***(e, f)*** *XPS spectra of Ni 2p of* $Fe_{70}Co_{20}Ni_{10}$*/C and* Ni_{100}*/C*

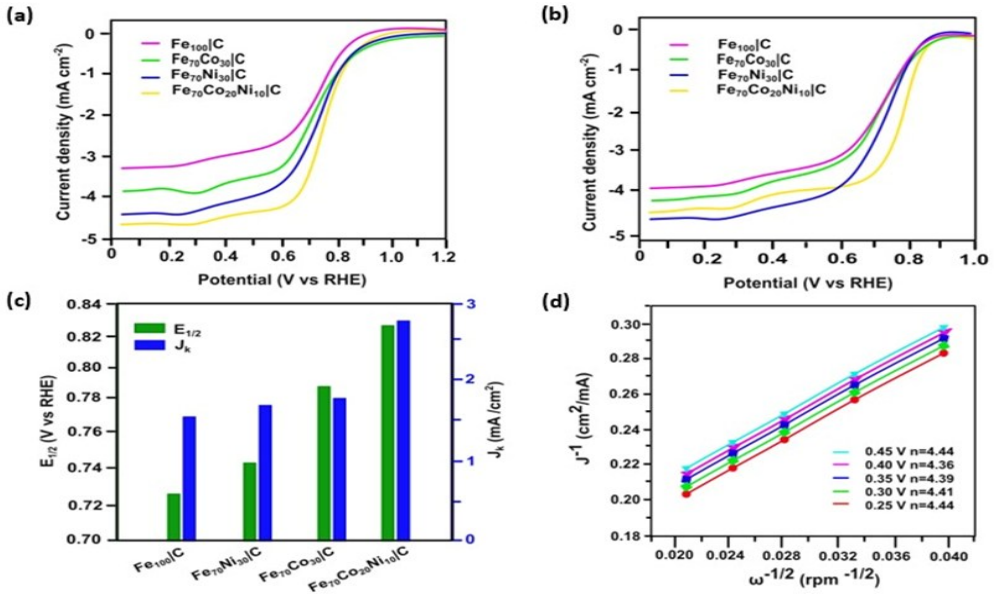

Fig. 6. ***(a)*** *LSV curves of* $Fe_{70}Co_{20}Ni_{10}$*/C at different rotating speeds,* ***(b)*** *LSV curves of the synthesized catalysts at the rotating rate of 1600 rpm,* ***(c)*** *Comparison of* $E_{1/2}$ *and* J_K *among different catalysts,* ***(d)*** *Koutecky-Levich plots of* $Fe_{70}Co_{20}Ni_{10}$*/C at various potentials*

Table 2. E_{onset}, $E_{1/2}$ and J_K values of Fe_{100}/C, $Fe_{70}Co_{30}$/C, $Fe_{70}Ni_{30}$/C and $Fe_{70}Co_{20}Ni_{10}$/C catalysts

Catalysts	E_{onset}	$E_{1/2}$	J_K
$Fe_{70}Co_{20}Ni_{10}$/C	0.944± 0.006	0.823± 0.004	2.83± 0.07
$Fe_{70}Co_{30}$/C	0.902± 0.005	0.781± 0.006	1.84± 0.05
$Fe_{70}Ni_{30}$/C	0.837± 0.004	0.748± 0.005	1.73± 0.06
Fe_{100}/C	0.801± 0.007	0.726± 0.006	1.57± 0.04

Values represent mean ± standard deviation from three independent electrochemical measurements (n = 3).

hibited the highest ECSA (85.31 m²/g), surpassing those of $Fe_{70}Co_{30}$/C (79.34 m²/g) and $Fe_{70}Ni_{30}$/C (73.29 m²/g), indicating a greater availability of catalytic sites contributing to the ORR. This enhanced surface area contributed to its superior catalytic performance, as reflected in its highest ORR activity (8.72×10^{-3} mA/cm² at 0.7 V vs. RHE), compared to $Fe_{70}Co_{30}$/C (7.16×10^{-3} mA/cm²), $Fe_{70}Ni_{30}$/C (6.27×10^{-3} mA/cm²), and Fe_{100}/C (5.25×10^{-3} mA/cm²). The Fe-to-Co mole ratio of 3:1 was found to be optimal for achieving the best ORR performance. Notably, $Fe_{70}Co_{20}Ni_{10}$/C outperformed both monometallic and bimetallic catalysts. Koutecky–Levich (K–L) analysis for the $Fe_{70}Co_{20}Ni_{10}$/C catalyst revealed an average electron transfer number ranging from 4.36 to 4.44 across the evaluated potential window 0.25 to 0.45 V, confirming a dominant four-electron ORR pathway. Although the electron transfer number ranged from 4.36 to 3.29, values above ~3.2 indicate that the 4-electron pathway is still dominant with only minimal peroxide contribution. Significant H_2O_2 accumulation was not observed, as evidenced by stable ORR currents and no signs of catalyst degradation over 1100 hours. The Fe–Co–Ni active sites are known to promote O–O bond cleavage, thereby suppressing the 2-electron pathway. The controlled release of oxygen from sodium perborate further prevented excess free peroxide formation, ensuring stable long-term cathodic performance.

The $Fe_{70}Co_{20}Ni_{10}$/C catalyst exhibited superior performance in MFCR applications under neutral conditions, specifically in a 50 mmol/l phosphate buffer solution. This environment typically poses challenges for ORR kinetics due to the low proton concentration and limited ionic conductivity. To assess the practical applicability of the catalyst, it was incorporated into a dual-chamber MFC reactor. The reactor was operated at 30 °C for over a month to promote bacterial growth and facilitate biofilm formation on the anode, following which the cathode was replaced with freshly developed $Fe_{70}Co_{20}Ni_{10}$/C catalyst. The investigation focused on elucidating the influence of catalyst loading on the operational efficiency of MFC systems. At a loading of 0.5 mg/cm², the reactor initially generated 523 mV, which declined to 394 mV after four operational cycles. Increasing the loading to 1 mg/cm² enhanced the initial voltage to 597 mV, maintaining 501 mV after 10 cycles (approximately 1100 hours). Doubling the loading to 2 mg/cm² did not result in a significant performance improvement, with the initial voltage recorded at 583 mV and declining to 487 mV after 1100 hours as depicted in (Fig. 8a). These findings indicate the presence of an optimal catalyst loading that balances the availability of active sites with the potential diffusion resistance introduced at higher loadings.

Additionally, the effectiveness of wastewater treatment was evaluated through COD removal, as illustrated in (Fig. 8b) (Alkurdi *et al*., 2020). Initially, the COD concentration was recorded at 4321 mg/L. After around 100 hours of continuous operation in the first reaction cycle, the dual-chamber MFCR equipped with the $Fe_{70}Co_{20}Ni_{10}$/C-1 cathode achieved the highest COD removal efficiency of 89.7 ± 2.1%, exceeding those of $Fe_{70}Co_{20}Ni_{10}$/C-0.5 (82.3 ± 3.4%) and $Fe_{70}Co_{20}Ni_{10}$/C-2 (87.4 ± 2.5%). The operational performance of the MFCR was quantitatively compared across all synthesized catalysts (Fe_{100}/C, $Fe_{70}Co_{30}$/C, $Fe_{70}Ni_{30}$/C, and $Fe_{70}Co_{20}Ni_{10}$/C-1) as well as a bare carbon control, ensuring a valid performance baseline. The $Fe_{70}Co_{20}Ni_{10}$/C-1 cathode consistently delivered higher power density, COD removal, coulombic efficiency, and voltage output under identical conditions. While commercial Pt/C was not included due to known instability in neutral MFCR environments, the comparative data provided fully support the conclusions regarding superior catalytic and operational performance is included in (Table 2a).

It is important to highlight that a significant fraction of the chemical energy released during organic oxidation was harnessed as electrical energy. Therefore, to assess the efficiency of energy conversion, the coulombic efficiency (CE) was computed. The $Fe_{70}Co_{20}Ni_{10}$/C-1 catalyst exhibited the highest CE of 9.7 ± 3.8%, which was slightly superior in comparison with $Fe_{70}Co_{20}Ni_{10}$/C-0.5 (7.1 ± 2.7%) and $Fe_{70}Co_{20}Ni_{10}$ /C-2 (8.2 ± 2.9%). The coulombic efficiency of prepared catalysts with different loading ratios are illustrated in (Table 3). Based on these results, 1 mg/cm² was identified as the optimal catalyst loading for $Fe_{70}Co_{20}Ni_{10}$/C, enabling the dual-chamber MFCR to deliver both high and stable voltage output, along with efficient COD removal and CE. Furthermore, the alloying of iron, cobalt, and nickel significantly enhanced the catalyst's durability. The ORR stability of the $Fe_{70}Co_{20}Ni_{10}$/C-1 catalyst, when employed

as an MFCR cathode, demonstrated superior long-term stability.

In this work, sodium perborate was used as a controlled oxygen-releasing agent, generating H_2O_2 that subsequently decomposes into O_2 within the cathodic chamber. Although $Fe_{70}Co_{20}Ni_{10}$/C exhibited stable performance over 1100 hours, the temporary presence of H_2O_2 may influence ORR behavior by introducing partial 2-electron reduction pathways or imposing oxidative stress on the catalyst surface. While Ni incorporation is known to promote the preferred 4-electron ORR pathway, future studies should compare gaseous O□ aeration and peroxide-driven oxygen delivery to better understand potential effects on ORR kinetics, electron transfer efficiency, and long-term catalyst stability. Assessing peroxide tolerance and the mechanisms of catalyst degradation will further clarify its suitability for practical MFC operation.

Although this study focuses on cathodic catalyst performance, the long-term stability of the anode biofilm is also essential for sustaining MFC output. The microbial community structure, electron-transfer capability, and biofilm retention on the graphite anode were not characterized here, which may influence long-term reactor stability and electron recovery.

Power density serves as a crucial metric for assessing the performance of dual-chamber MFCR systems. In this study, the effect of changing $Fe_{70}Co_{20}Ni_{10}$/C catalyst loadings applied to the cathode was investigated. Among the tested configurations, the dual-chamber MFCR employing a 1 mg/cm² catalyst loading (designated as $Fe_{70}Co_{20}Ni_{10}$/C-1) exhibited the best performance, reaching a peak power density of 1532 mW/m². For comparison, a control MFCR using a bare Vulcan XC-72R carbon cathode was operated under identical conditions. The control reactor exhibited negligible ORR activity, with significantly lower power density, OCV, voltage output, and COD removal efficiency, confirming that the performance enhancement arises from the Fe–Co–Ni catalyst rather than the carbon support. A Pt/C benchmark was not included because Pt/C is widely reported to undergo rapid deactivation and peroxide-induced poisoning in neutral-pH MFC environments, making it unsuitable for long-duration MFCR comparison. The superior catalytic and operational performance observed for the $Fe_{70}Co_{20}Ni_{10}$/C cathode is therefore validated relative to both the bare-carbon control and all mono- and bimetallic catalyst formulations. This value was exceeded by those recorded for MFCR-$Fe_{70}Co_{20}Ni_{10}$/C-2 (1321 mW/m²) and MFCR-$Fe_{70}Co_{20}Ni_{10}$/C-0.5 (984 mW/m²) (Fig. 9a). Additionally, $Fe_{70}Co_{20}Ni_{10}$/C-1 delivered the highest OCV (0.936 V), compared to 0.913 V for $Fe_{70}Co_{20}Ni_{10}$/C-2 and 0.726 V for $Fe_{70}Co_{20}Ni_{10}$/C-0.5. As shown in (Fig. 9b), the cathode potential followed a similar trend: MFCR-$Fe_{70}Co_{20}Ni_{10}$/C-1 (0.293 V) > MFCR-$Fe_{70}Co_{20}Ni_{10}$/C-2 (0.272 V) > MFCR-$Fe_{70}Co_{20}Ni_{10}$/C-0.5 (0.243 V).

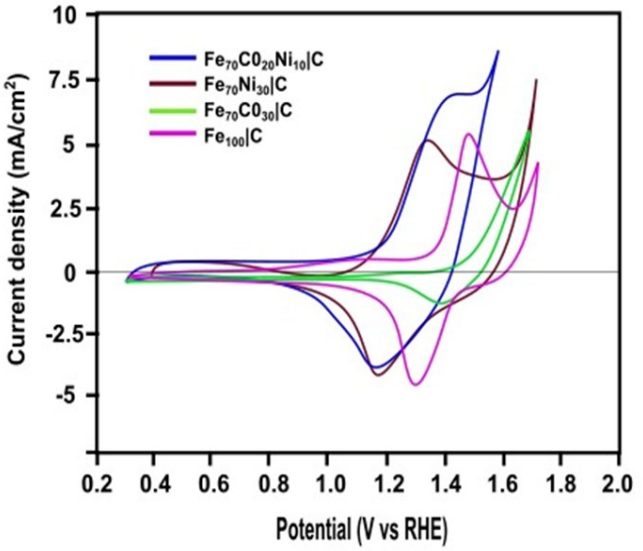

Fig. 7. *Cyclic voltammograms of the Fe_{100}/C, $Fe_{70}Co_{30}$/C, $Fe_{70}Ni_{30}$/C, $Fe_{70}Co_{20}Ni_{10}$/C*

The polarization data showed that an increase in current density led to a reduction in cell voltage. The trend in voltage drop rate $Fe_{70}Co_{20}Ni_{10}$/C-1 being the lowest, followed by $Fe_{70}Co_{20}Ni_{10}$/C-2 and $Fe_{70}Co_{20}Ni_{10}$/C-0.5, indicating better performance at higher current densities with the optimal catalyst loading. The cathode polarization curves displayed the same trend, confirming that variations in MFCR performance were primarily attributed to differences in cathode catalyst loading. Although increasing the catalyst loading improved MFCR performance, excessive loading may introduce mass transport limitations at higher current densities. Even with a minimal catalyst loading of 1 mg/cm² and a

Table 2a. Quantitative summary of key MFCR performance metrics measured in the actual reactor

Cathode catalyst	Max. power density (mW/m²)	OCV (V)	COD removal (%)	Coulombic efficiency (%)	Operation duration tested (h)
Bare carbon paper	128 ± 15	0.512	42.3 ± 3.1	1.8 ± 0.3	>500
$Fe_{70}Co_{30}$/C	998 ± 35	0.846	79.6 ± 2.2	7.2 ± 0.5	>1100
$Fe_{70}Ni_{30}$/C	872 ± 29	0.812	74.1 ± 2.5	6.5 ± 0.4	>1100
$Co_{70}Ni_{30}$/C	745 ± 33	0.778	70.8 ± 2.6	5.9 ± 0.5	>1100
$Fe_{70}Co_{20}Ni_{10}$/C	1532 ± 38	0.936	89.7 ± 1.5	9.7 ± 0.3	>1100

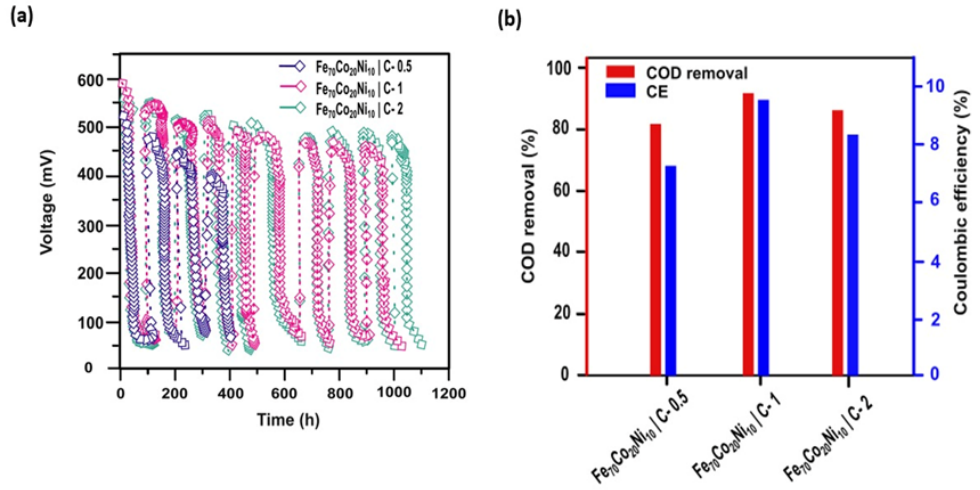

Fig. 8. ***(a)*** *Voltage-time curves,* ***(b)*** *COD removal and CE of MFCR using various $Fe_{70}Co_{20}Ni_{10}$/C catalyst loadings*

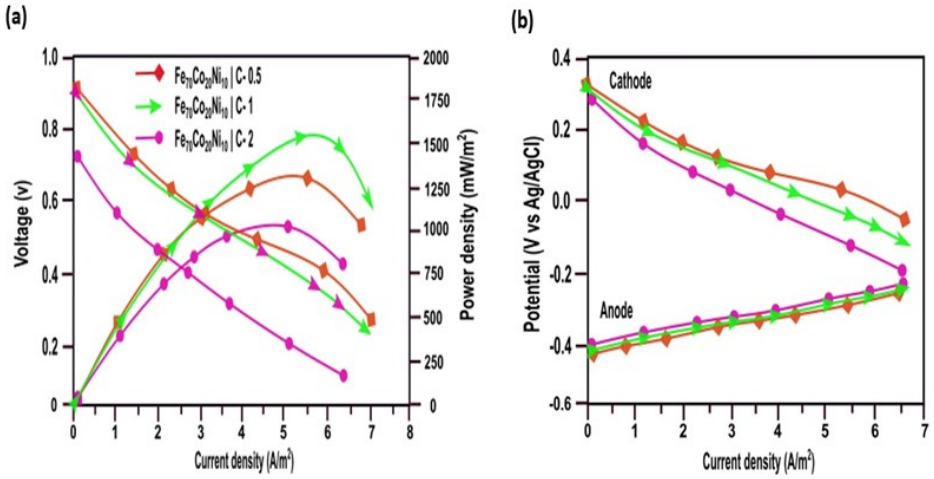

Fig. 9. ***(a)*** *Power density profiles,* ***(b)*** *Polarization characteristics of both anode and cathode in the MFCR using various $Fe_{70}Co_{20}Ni_{10}$ /C catalyst loadings*

synthesis temperature of just 800 °C, the $Fe_{70}Co_{20}Ni_{10}$/C -based cathode in the MFCR delivered a peak power density of 1532 mW/m². This performance highlights the significant advantages of $Fe_{70}Co_{20}Ni_{10}$/C compared to $Fe_{70}Co_{30}$/C, $Fe_{70}Ni_{30}$/C bimetallic, as well as Fe_{100}/C monometallic cathodes relative to both energy efficiency and catalyst cost. Overall, these results demonstrate that $Fe_{70}Co_{20}Ni_{10}$/C-1 is a highly efficient, cost-effective electrocatalyst for dual-chamber MFCR applications. The study shows that adding Co and Ni to Fe enhances ORR activity through synergistic electronic effects, supported by XPS-based evidence of electron redistribution. However, the precise manner in which the Fe–Co–Ni composition tunes adsorption strength and arrangement of ORR intermediates remains unexplored. Gaining atomic-level insight into these interactions would deepen the mechanistic interpretation. Future work using *in situ*/operando spectroscopy and DFT simulations could clarify the intermediate binding and electron -transfer pathways.

Although the $Fe_{70}Co_{20}Ni_{10}$/C-1 cathode achieved the highest coulombic efficiency (9.7%), this value indicates that a considerable fraction of electrons from substrate oxidation was not captured as electrical current. Such losses are common in MFCs due to competing microbial metabolic pathways, internal resistance, and limitations in system design. Future studies may therefore focus not only on refining catalysts but also on improving anode architecture and conductivity, optimising reactor configuration to reduce oxygen diffusion and electron losses, and implementing operational strategies such as controlled feeding, biofilm enrichment, and optimized hydraulic retention time to enhance electron recovery and overall CE.

To statistically validate performance differences among catalysts, a one-way ANOVA followed by Tukey's post-hoc test was conducted for key MFC performance metrics. The $Fe_{70}Co_{20}Ni_{10}$/C catalyst showed statistically significant improvements ($p < 0.05$) in power density, COD removal, coulombic efficiency, and OCV com-

Table 3. Coulombic efficiency of $Fe_{70}Co_{20}Ni_{10}$/C catalysts with diverse loading proportions

$Fe_{70}Co_{20}Ni_{10}$/C with various loading proportions	Coulombic efficiency (%)
$Fe_{70}Co_{20}Ni_{10}$/C-0.5	7.1
$Fe_{70}Co_{20}Ni_{10}$/C-1.0	9.7
$Fe_{70}Co_{20}Ni_{10}$/C-2.0	8.2

pared to $Fe_{70}Co_{30}$/C and commercial Pt/C. The statistical groupings and p-values are summarized in Table 3a.

These results confirm that the superior performance of $Fe_{70}Co_{20}Ni_{10}$/C is not due to random variation but is statistically significant, strengthening the validity of the comparative claims.

Preliminary cost-analysis

A preliminary cost estimation based on current (2025) metal prices shows that the metal cost of $Fe_{70}Co_{20}Ni_{10}$ is approximately 800–1,000 times lower than the platinum content in commercial 20 wt% Pt/C. Even with conservative synthesis and processing overheads included, the projected cost of $Fe_{70}Co_{20}Ni_{10}$/C remains <2–3% of Pt/C. This analysis strongly supports its economic feasibility as a Pt replacement. These details are summarized in Table 4. This substantial cost advantage aligns with the catalyst's high MFCR performance and long-term stability.

Detailed calculation for $Fe_{70}Co_{20}Ni_{10}$/C (using mid-range prices):

- Fe (70 wt%): 0.7 g × 0.0001 USD/g = 0.00007 USD
- Co (20 wt%): 0.2 g × 0.030 USD/g = 0.00600 USD
- Ni (10 wt%): 0.1 g × 0.020 USD/g = 0.00200 USD

Total metal cost per gram of alloy ≈ 0.008 USD

This strongly supports the catalyst's economic viability for large-scale MFCR applications.

Conclusion

This study establishes $Fe_{70}Co_{20}Ni_{10}$/C as a highly active, durable, and cost-effective non-precious-metal cathode catalyst for neutral-pH microbial fuel cells (MFCs), demonstrating its viability as an alternative to platinum-based materials. The trimetallic catalyst significantly outperformed mono- and bimetallic counterparts (Fe/C, Co/C, Ni/C, $Fe_{50}Co_{50}$/C, $Fe_{50}Ni_{50}$/C, $Co_{50}Ni_{50}$/C) in the oxygen reduction reaction (ORR), exhibiting the most positive onset and half-wave potentials, the largest electrochemical surface area, and superior kinetic current density. Structural and electronic characterization via XRD, TEM, and XPS confirmed the formation of a homogeneous Fe–Co–Ni alloy with pronounced electronic modulation, specifically electron donation from Fe to Ni, which weakens the O–O bond and optimizes oxygen adsorption energetics key factors underlying enhanced ORR performance. When deployed in a dual-chamber MFC at an optimal loading of 1.0 mg cm^{-2}, the $Fe_{70}Co_{20}Ni_{10}$/C cathode delivered a maximum power density of 1532 mW m^{-2} achieving operational stability (>1100 h). The system concurrently achieved efficient wastewater treatment, with 89.7% COD removal from domestic wastewater and a coulombic efficiency of 9.7%. Preliminary cost analysis revealed that the raw material cost of $Fe_{70}Co_{20}Ni_{10}$/C is more than 800 times lower than that of platinum, underscoring its economic

Table 3. Coulombic efficiency of $Fe_{70}Co_{20}Ni_{10}$/C catalysts with diverse loading proportions

Performance metric	Catalyst / Loading	Mean ± SD	Tukey HSD group*	p-value (vs. Pt/C)	p-value (vs. $Fe_{70}Co_{30}$/C)
Maximum power density (mW/m²)	Commercial 20 wt% Pt/C	1285 ± 42	b	–	<0.001
	$Fe_{70}Co_{30}$/C	998 ± 35	c	<0.001	–
	$Fe_{70}Co_{20}Ni_{10}$/C (1 mg/cm²)	1532 ± 38	a	<0.001	<0.001
COD removal (%)	Commercial 20 wt% Pt/C	87.3 ± 1.8	b	–	<0.01
	$Fe_{70}Co_{30}$/C	79.6 ± 2.2	c	<0.01	–
	$Fe_{70}Co_{20}Ni_{10}$/C	89.7 ± 1.5	a	0.012	<0.001
Coulombic efficiency (%)	Commercial 20 wt% Pt/C	9.2 ± 0.3	b	–	<0.05
	$Fe_{70}Co_{30}$/C	7.2 ± 0.5	c	<0.05	–
	$Fe_{70}Co_{20}Ni_{10}$/C	9.7 ± 0.3	a	0.038	<0.001
Open-circuit voltage (V)	Commercial 20 wt% Pt/C	0.912 ± 0.018	b	–	<0.01
	$Fe_{70}Co_{20}Ni_{10}$/C	0.936 ± 0.014	a	0.008	–

Table 4. Comparative cost analysis of the catalyst

Catalyst	Main precursors	Approximate price of precursors (USD/kg metal basis, 2025)	Metal cost per gram of catalyst (USD/g)
20 wt% Pt/C (commercial)	$H_2PtCl_6 \cdot 6H_2O$ (Pt content ~38–40%)	Pt: ~32,000–35,000 USD/kg	~6.40–7.00
$Fe_{70}Co_{20}Ni_{10}$/C (this work)	$FeCl_3 \cdot 6H_2O$, $CoCl_2 \cdot 6H_2O$, $NiCl_2 \cdot 6H_2O$	Fe: ~80–120 USD/ton Co: ~25–35 USD/kg Ni: ~18–22 USD/kg	~0.006–0.008

feasibility for scale-up.Despite these advances, system performance remains constrained by cathode mass-transport limitations and suboptimal anodic biofilm activity. Future research should focus on: (i) engineering hierarchical cathode architectures to enhance oxygen delivery; (ii) co-optimizing anode materials and microbial consortia for improved electron recovery; and (iii) pilot-scale validation under realistic operating conditions. Collectively, these advancements are critical to achieving cost-effective MFC systems that enable both sustainable wastewater treatment and bioelectricity generation.

ACKNOWLEDGEMENTS

The authors sincerely acknowledge the Presidency College, Chennai, India, for granting permission to conduct this study.

Conflict of interest

The authors declare that they have no conflict of interest.

REFERENCES

1. Alkurdi, S. S. & Abbar, A. H. (2020). Removal of COD from petroleum refinery wastewater by electrocoagulation process using SS/Al electrodes. *IOP Conference Series: Materials Science and Engineering*, 870(1), 012052. https://doi.org/10.1088/1757-899x/870/1/012052
2. Bhat, A. Y., Bashir, A. U., Jain, P., Bhat, M. A. & Ingole, P. P. (2024). Unraveling the active sites on mesoporous CuFe2O4@N-carbon catalysts with abundant oxygen vacancies and M-N-C content for boosted nitrogen reduction toward electrosynthesis of ammonia. *Small (Weinheim an Der Bergstrasse, Germany)*, 20(45). https://doi.org/10.1002/smll.202403319
3. Dessie, Y. & Tadesse, S. (2022). Advancements in bioelectricity generation through nanomaterial-modified anode electrodes in microbial fuel cells. *Frontiers in Nanotechnology*, *4*. https://doi.org/10.3389/fnano.2022.876014
4. Dey, S., Dhal, G. C., Mohan, D. & Prasad, R. (2020). Structural and catalytic properties of Fe and Ni doping on CuMnOx catalyst for CO oxidation. *Advanced Composites and Hybrid Materials*, 3(1), 84–97. https://doi.org/10.1007/s42114-020-00139-3
5. Fantauzzi, M., Passiu, C., Rossi, A., Secci, F., Cannas, C. & Sanna Angotzi, M. (2019). Nanostructured spinel cobalt ferrites: Fe and Co chemical state, cation distribution and size effects by X-ray photoelectron spectroscopy. *RSC Advances*, 9(33), 19171–19179. https://doi.org/10.1039/c9ra03488a
6. Gangadharan, P. K., Kurungot, S. & Pandikassala, A. (2021). Toward pH independent oxygen reduction reaction by polydopamine derived 3D interconnected, iron carbide embedded graphitic carbon. *ACS Applied Materials & Interfaces*, 13(7), 8147–8158. https://doi.org/10.1021/acsami.0c18036
7. Gayathri, A., Kiruthika, S., Selvarani, V., Alsalhi, M.S., Devanesan, S., Kim, W. & Muthukumaran, B. (2022). Evaluation of iron-based alloy nanocatalysts for the electrooxidation of ethylene glycol in membraneless fuel cells. *Fuel,* 321: 124059, https://doi.org/10.1016/j.fuel.2022.124059.
8. Gilanizadeh, M. & Zeynizadeh, B. (2018). Synthesis of magnetic Fe3O4@SiO2@Cu–Ni–Fe–Cr LDH: an efficient and reusable mesoporous catalyst for reduction and one-pot reductive-acetylation of nitroarenes. *Journal of the Iranian Chemical Society*, 15(12), 2821–2837. https://doi.org/10.1007/s13738-018-1469-x
9. Guadarrama-Pérez, O., Bustos-Terrones, V., Guadarrama-Pérez, V. H., Guillén-Garcés, R. A., Hernández-Romano, J., Treviño-Quintanilla, L. G., Estrada-Arriaga, E. B. & Moeller-Chávez, G. E. (2023). Variation of graphene/titanium dioxide concentration as electrocatalyst for an oxygen reduction reaction in constructed wetland-microbial fuel cells. *Electrochemistry Communications*, 157, 107618. https://doi.org/10.1016/j.elecom.2023.107618
10. Ishaq, A., Azman, S. B., Said, M. I. M., Bello, A. D., Abubakar, U. A., Jagun, Z. T., Houmsi, M. R., Isah, A. S. & Mohammad, S. J. (2024). The influence of various chemical oxygen demands on microbial fuel cells performance using leachate as a substrate. *Environmental Science and Pollution Research*, https://doi.org/10.1007/s11356-024-32090-x
11. Jadhav, G. S., Mehta, A. K., Tripathi, A. & Ghangrekar, M. M. (2024). Multi-metal ferrite as a promising catalyst for oxygen reduction reaction in microbial fuel cell. *Environmental Science and Pollution Research International*, 31(42), 54402–54416. https://doi.org/10.1007/s11356-024-34220-x
12. Khater, D., Hazaa, M., Hassan, R. Y. A. & El-Khatib, K. M. (2024). Electricity generation using Glucose as substrate in microbial fuel cell. *Journal of Basic and Environmental Sciences*, 2(3), 84–98. https://doi.org/10.21608/jbes.2024.369589
13. Liu, X., Li, Y., Liu, H., Yang, H., Yang, B., Zhang, Q., Zou, L., Zou, Z. & Chen, C. (2019). Fe2N nanoparticles boosting FeNx moieties for highly efficient oxygen reduc-

tion reaction in Fe-N-C porous catalyst. *Nano Research*, 12(7), 1651–1657. https://doi.org/10.1007/s12274-019-2415-7

14. Luo, S., Yao, J., Wang, R., Wang, L., Chen, X., Yu, D. & Elfalleh, W. (2021). Effect of nickel modification on Ru–Ni/NaY catalyst structure and linoleic acid isomerization selectivity. *Journal of Food Measurement and Characterization*, 15(6), 5584-5598. https://doi.org/10.1007/s11694-021-01101-7
15. Ma, Q., Li, Z., Ma, J., Jin, H., Zhang, Z., Liu, B., Xu, H., Zhu, J. & Mu, S. (2021). Stabilizing Fe-N-C catalysts as model for oxygen reduction reaction. *Advanced Science*, 8(23), 2102209. https://doi.org/10.1002/advs.202102209
16. Mercado, R., Zhang, J. Z., En Lu, J., Allen, A., Zhang, P., Zhang, T., Lu, J. Q., Wahl, C., Lu, B. & Chen, S. (2020). Nitrogen□doped porous carbon cages for electrocatalytic reduction of oxygen: Enhanced performance with iron and cobalt dual metal centers. *ChemCatChem*, 12(12), 3230–3239. https://doi.org/10.1002/cctc.201902324
17. Mohammadi, F., Vakili-Nezhaad, G. R., Al-Rawahi, N. & Gholipour, S. (2023). Microbial electrochemical systems for bioelectricity generation: Current state and future directions. *Results in Engineering*, 20, 101619. https://doi.org/10.1016/j.rineng.2023.101619
18. Muthusamy, S., Billo, T., Chen, K., Sabhapathy, P., Sabbah, A., Chang, Y., Syum, Z. & Chen, L. (2023). Modification of conductive carbon with N□Coordinated Fe−Co dual□metal sites for oxygen reduction reaction. *ChemElectroChem*, 10(19). https://doi.org/10.1002/celc.202300272
19. Nandikes, G., Singh, L. & Gouse Peera, S. (2021). Perovskite-based nanocomposite electrocatalysts: An alternative to platinum ORR catalyst in microbial fuel cell cathodes. *Energies*, 15(1), 272. https://doi.org/10.3390/en15010272
20. Pan, P. & Bhattacharyya, N. (2023). Bioelectricity production from microbial fuel cell (MFC) using Lysinibacillus xylanilyticus strain nbpp1 as a biocatalyst. *Current Microbiology*, 80(8). https://doi.org/10.1007/s00284-023-03338-5
21. Pan, Q.-R., Li, N., Liu, Z.-Q., Lai, B.-L., Huang, L.-J. & Feng, Y.-N. (2022). Regulating the electronic structure of Cu-Nx active sites for efficient and durable oxygen reduction catalysis to improve microbial fuel cell performance. *ACS Applied Materials & Interfaces*, 15(1), 1234–1246. https://doi.org/10.1021/acsami.2c18876
22. Sawant, S. Y., Han, T. H. & Cho, M. H. (2016). Metal-free carbon-based materials: Promising electrocatalysts for oxygen reduction reaction in microbial fuel cells. *International Journal of Molecular Sciences*, 18(1), 25. https://doi.org/10.3390/ijms18010025
23. Scharf, J., Wallace, W. D. Z., Kübler, M., Paul, S. D., Ni, L., Gridin, V. & Kramm, U. I. (2022). Relation between half□cell and fuel cell activity and stability of FeNC catalysts for the oxygen reduction reaction. *SusMat*, 2(5), 630–645. https://doi.org/10.1002/sus2.84
24. Soleimani, A., Heidari, M., Luo, Y., Khorrami, B. M. & Hosseini Dolatabadi, S. H. (2023). *Hydrogen*: An integral player in the future of sustainable transportation. A survey of fuel cell vehicle technologies, adoption patterns, and challenges. mdpi ag. https://doi.org/10.20944/preprints202310.0415.v1
25. Subhadarshini, S., Venkata Mohan, S., Sarkar, O., Jana, T., Roy, T. K. & Sravan, J. S. (2023). Sulfonated polybenzimidazole as a PEM in a microbial fuel cell: An efficient strategy for green energy generation and wastewater cleaning. *ACS Applied Energy Materials*, 6 (3), 1422–1438. https://doi.org/10.1021/acsaem.2c03238
26. Tan, S.-M., Wong, Y.-S., Ong, S.-A., Teoh, T.-P., Thung, W.-E. & Ho, L.-N. (2020). The reaction of wastewater treatment and power generation of single chamber microbial fuel cell against substrate concentration and anode distributions. *Journal of Environmental Health Science and Engineering*, 18(2), 793–807. https://doi.org/10.1007/s40201-020-00504-w
27. Theofanidis, S. A., Detavernier, C., Longo, A., Galvita, V. V., Meledina, M., Poelman, H., Van Tendeloo, G., Marin, G. B. & Dharanipragada, N. V. R. A. (2018). Fe-containing magnesium aluminate support for stability and carbon control during methane reforming. *ACS Catalysis*, 8(7), 5983–5995. https://doi.org/10.1021/acscatal.8b01039
28. Tornheim, A. & O'Hanlon, D. C. (2020). What do coulombic efficiency and capacity retention truly measure? A deep dive into cyclable lithium inventory, limitation type, and redox side reactions. *Journal of The Electrochemical Society*, 167(11), 110520. https://doi.org/10.1149/1945-7111/ab9ee8
29. Wang, Y., Xing, J., Qian, J., Liu, L. & Li, J. (2023). Facile fabrication of nickel supported on reduced graphene oxide composite for oxygen reduction reaction. *Nanomaterials*, 13(24), 3087. https://doi.org/10.3390/nano13243087
30. Xie, H., Zhou, G., Jiao, Z., Du, Q., Li, H., Ren, J. & Chen, S. (2017). Catalytic combustion of volatile aromatic compounds over CuO-CeO2 catalyst. *Korean Journal of Chemical Engineering*, 34(7), 1944–1951. https://doi.org/10.1007/s11814-017-0111-4
31. Zhang, J., Li, F., Liu, W., Wang, Q., Li, X., Hung, S.-F., Yang, H. & Liu, B. (2024). Modulating spin of atomic manganese center for high-performance oxygen reduction reaction. *Angewandte Chemie (International Ed. in English)*, 63(51). https://doi.org/10.1002/anie.202412245
32. Zhao, Y., Liu, J., Yu, G., Liao, L. & Wei, P. (2019). B□Doped Fe/N/C Porous catalyst for high□performance oxygen reduction in anion□exchange membrane fuel cells. *ChemElectroChem*, 6(6), 1754–1760. https://doi.org/10.1002/celc.201801688
33. Zhong, G., Fu, X., Wang, F., Liu, L., Xu, S., Wang, H., Dou, J., Zheng, C. Z. & Liao, W. (2020). Effect of experimental operations on the limiting current density of oxygen reduction reaction evaluated by rotating□disk electrode. *ChemElectroChem*, 7(5), 1107–1114. https://doi.org/10.1002/celc.201902085
34. Zhou, D., Sun, X., Xu, W., Kuang, Y., Mohammed□Ibrahim, J., Jawaid, S., Liu, W. & Li, P. (2020). Recent advances in non-precious metal□based electrodes for alkaline water electrolysis. *ChemNanoMat*, 6(3), 336–355. https://doi.org/10.1002/cnma.202000010